

Article

## Empirical Equation Based Chirality ( $n, m$ ) Assignment of Semiconducting Single Wall Carbon Nanotubes from Resonant Raman Scattering Data

Md Shamsul Arefin

Department of Electrical Engineering and Computer Science, Northern Arizona University, South San Francisco Street, Flagstaff, AZ 86011, USA; E-Mail: msa59@nau.edu; Tel.: +1-928-814-5931; Fax: +1-928-523-2300.

Received: 2 November 2012; in revised form: 30 November 2012 / Accepted: 6 December 2012 / Published: 24 December 2012

---

**Abstract:** This work presents a technique for the chirality ( $n, m$ ) assignment of semiconducting single wall carbon nanotubes by solving a set of empirical equations of the tight binding model parameters. The empirical equations of the nearest neighbor hopping parameters, relating the term  $(2n - m)$  with the first and second optical transition energies of the semiconducting single wall carbon nanotubes, are also proposed. They provide almost the same level of accuracy for lower and higher diameter nanotubes. An algorithm is presented to determine the chiral index ( $n, m$ ) of any unknown semiconducting tube by solving these empirical equations using values of radial breathing mode frequency and the first or second optical transition energy from resonant Raman spectroscopy. In this paper, the chirality of 55 semiconducting nanotubes is assigned using the first and second optical transition energies. Unlike the existing methods of chirality assignment, this technique does not require graphical comparison or pattern recognition between existing experimental and theoretical Kataura plot.

**Keywords:** chiral index; chirality assignment; single wall carbon nanotube; resonant Raman spectroscopy; optical transition energy; tight-binding model; nearest-neighbor hopping parameter

---

## 1. Introduction

Semiconducting single wall carbon nanotubes (SWCNTs) already emerged as a promising candidate for photovoltaic applications [1–6], opto-electronics [7,8], and molecular electronics [9–11]. A number of advanced applications such as transistor memory [9], field-effect transistors [10], and near-infrared optical sensors [11] require nanotube samples with little or no structural variation. A SWCNT  $(n, m)$  is metallic if  $\text{mod}(n - m, 3) = 0$  and semiconducting if  $\text{mod}(n - m, 3) = 1$  or  $2$  (commonly termed as mod 1 or mod 2 type, respectively) [12]. This relation is always found true except for SWCNT with a very small diameter, where curvature effect dominates its properties [13]. Since the electronic and the optical properties of SWCNT vary greatly with their chirality, the experimental determination of the chirality  $(n, m)$  of SWCNT has been a challenge ever since their discovery [14,15]. Identification of spectroscopic features and correlating them with nanotube geometric structure is always necessary to separate, sort, and identify nanotubes after their production [12,16]. Methods including dielectrophoresis [17,18], centrifugation [19–21], chromatography [22–24], selective solubilization [25,26], and selective reaction [27,28] are devised for the separation and sorting of semiconducting SWCNTs from metallic nanotubes. After the separation, the immediate next challenge is to identify the chiral index  $(n, m)$  of each semiconducting SWCNT. As the fabrication techniques are not yet in the position to deliver nanotubes of specific chirality, there is still a need for reliable techniques for the identification of the chirality of a given nanotube.

Since the diameter of an individual SWCNT is determined by its chirality,  $(n, m)$ , there have been a number of experimental approaches based on TEM [29], STM [30,31], or the radial breathing mode (RBM) in Raman spectroscopy [15,16] to determine the diameter of a given nanotube. In principle, an exact knowledge of the diameter allows the determination of the chiral indices of a tube. However, the diameters are a multi-valued function of chirality  $(n, m)$  and are too closely spaced for such a procedure to work. Moreover, as two different SWCNTs may have the same diameter, the unique assignment of chirality only from the diameter is impossible. Hence, at least one more piece of information is required for unique assignment of the chirality of nanotube [15].

Resonant Raman scattering (RRS) [15,16,32–43], Rayleigh scattering [44–48], and photoluminescence (PL) excitation [49–53] have been the mainstream tools for non-destructive chirality characterization, and each method has unique capabilities. Each method uses at least two pieces of information for the unique assignment of chirality [37,41,42]. First, RRS method uses one optical transition energy,  $(E_{ii})$  and the nanotube RBM frequency,  $\omega_{rbm}$ . Second, Rayleigh scattering uses electron diffraction. Lastly, PL method uses optical absorption and emission energies for unique chirality assignment [37]. Bachilo *et al.* [50] showed PL based effective chirality  $(n, m)$  assignment based on pattern recognition between experimental and theoretical (derived from the extended tight binding model) plot of the second transition (excitation) energy versus the first transition (emission) energy. It can be noted that all these methods commonly use the information about one of the transition energies. Though the spectroscopic experiments are different in these methods, they bear some similarities in principle. All of them follow a laborious mapping of the observed properties of the produced batch of SWCNTs with an existing theoretical plot that depicts the same properties to find one-to-one correspondence of chirality. Therefore, the methods need to go through some kind of

pattern recognition process and need a prior graphical plot to make final assignment. Moreover, pattern recognition is possible simply if the Raman spectrum shows a set of different RBMs. This is merely the case for samples containing different kinds of nanotubes that are produced as ensembles of nanotubes. There is no scope for pattern recognition, if all observed Raman spectra shows just one RBM for an isolated tube or if the sample contains only one kind of chiral indices  $(n, m)$ . In such case, quality of the assignment fully depends on the chosen theoretical plot and may lead to ambiguity.

RRS is quite reliable, straightforward (though laborious and expensive), and hence most widely used for chiral index assignment. Moreover, RRS can be performed in resonance with the second optical transition, which is in the visible energy range. Thus, no infrared-sensitive spectrometers and detectors are needed [37]. RRS provides the information of the optical transition energies ( $E_{ii}$ ) and the RBM frequency ( $\omega_{rbm}$ ). The RBM frequency gives the diameter ( $d_t$ ) as they are inversely related through a semi-empirical equation [16,33,34,50,54,55]. Since the  $(E_{ii}, \omega_{rbm})$  pair is unique for each SWCNT, proper structural assignment can be made using a prior theoretical model for  $(E_{ii}, \omega_{rbm})$  to  $(n, m)$  transformation [42]. Earlier approach was to plot all  $E_{ii}$  versus  $d_t$  (from  $\omega_{rbm}$ ) to form an experimental Kataura plot that is mapped with an existing theoretical Kataura plot to give one-to-one correspondence for each chirality [32,33]. Unfortunately, the uniqueness of this transformation may be hampered in this process by the possible error involved in the empirical calculation of  $d_t$  from  $\omega_{rbm}$ . Hence, alternative methods were proposed later by many authors where all  $E_{ii}$  are plotted directly against corresponding  $\omega_{rbm}$  [42,43] or inverse  $\omega_{rbm}$  [15,36,37] (instead of  $d_t$ ) and compared with a theoretical plot of  $(E_{ii}, \omega_{rbm})$  or  $(E_{ii}, 1/\omega_{rbm})$ . Then pattern recognition between two plots is performed by stretching and shifting the vertical and horizontal axes of the plots until good correspondence between the experimental points and the theoretically calculated values is achieved [15,36,37]. By this process, assumption of empirical parameters for calculating  $d_t$  from  $\omega_{rbm}$  can be avoided and possible theoretical or experimental error can be neutralized within a limit. Though this pattern recognition finally gives a unique one-to-one correspondence for each chiral index  $(n, m)$ , it requires to follow the pattern recognition approach and also needs a prior graphical plot or tabulated data.

This paper presents an empirical equation based novel technique for SWCNT chirality assignment where the chiral index  $(n, m)$  can be directly found by solving the empirical equations of the nearest neighbor hopping parameters. So far, no such equation based technique is proposed for chirality assignment. Like other methods, it also requires the information of optical transition energy and nanotube diameter ( $d_t$ ). However, unlike other methods, it does not follow graphical approach and does not need a prior tabulated data or graphical plot. This method is applicable for any semiconducting SWCNT, whether isolated or in a batch.

The remainder of this article is organized as follows. A set of Empirical equations of the nearest neighbor hopping parameters for calculating the first and second optical transition energies are formulated in Section 2. Section 3 describes the proposed empirical equation based chirality assignment technique using both the first optical transition energy and the second optical transition energy. The empirical equations are used from reverse direction for chirality assignment. An algorithm to determine the chiral index  $(n, m)$  of unknown SWCNT from RRS experiment is also discussed. The supporting empirical equations for calculating chiral indexes are presented in Appendix A and B. The numerical results for chirality assignment of 28 semiconducting tubes using the first optical transition energy and

the RBM frequency values and 27 semiconducting tubes using the second optical transition energy and the RBM frequency values are presented in Section 4. Finally, Section 5 presents the conclusions.

## 2. Modified Tight Binding Model

In this section, a set of empirical equations are formulated that can predict the first ( $E_{11}$ ) and second ( $E_{22}$ ) optical transition energies accurately. This section serves as the first step of empirical equation based chirality assignment. In the next section, the empirical equations that are used from reversed direction for chirality assignment are presented.

The simple expression [45] of optical transition energies from Tight Binding model with the nearest-neighbor approximation is

$$E_{ii} = 2j\gamma_0 a_{cc}/d_t \quad (1)$$

where  $\gamma_0$  is the nearest-neighbor hopping parameter,  $a_{cc} = 0.144$  nm is carbon-carbon bond length,  $d_t$  is nanotube diameter in nm, given by  $d_t = \sqrt{3(n^2 + nm + m^2)}a_{cc}/\pi$ , and  $n$  is an integer. This equation gives first optical transition energy for  $i = 1, j = 1$ ,

$$E_{11} = \frac{2\gamma_0 a_{cc}}{d_t} \quad (2)$$

Since the experimental observation showed that the ratio of  $E_{22}$  to  $E_{11}$  deviates from 2, the ratio is termed as “ $r$ ” [56]. Putting  $i = 2, j = r$  in Equation (1) gives the expression of second optical transition energy ( $E_{22}$ ) as,

$$E_{22} = \frac{2r\gamma_0 a_{cc}}{d_t} \quad (3)$$

Equation (1) shows good qualitative agreement with experimental results but fails quantitatively [57–59]. This is because, it originates from a too simple model of SWCNT that ignores important experimental observations like “curvature effect”, “chirality effect”, “trigonal warping effect”, and “many body effect” (electron-electron interaction) [60–64]. The first factor, “Curvature effect”, is induced by  $\sigma$ - $\pi$  re-hybridization and de-localized  $\pi$ -bond orbitals and corresponding band structure deviation from simple  $\pi$ -orbital graphene picture [13,57,59–61]. It causes quantitative difference and also turns some  $\text{mod}(n - m, 3) = 0$  tubes into quasi-metallic or small bandgap semiconductors [59]. The effect is stronger for small diameter tubes due to their bigger curvature [59]. Since diameter  $d_t$  is fully responsible for tube curvature, suitable inclusion of  $d_t$  term can reflect this effect. The second factor is “chirality effect” that originates from individual nanotube chirality and responsible for some unique features of each tube. As classifying semiconducting SWCNT in mod 1 and mod 2 type originates from chirality ( $n, m$ ), not from chiral angle, chirality effect can be reflected through alternative combination of chiral index. The third factor is “trigonal warping effect” [64,65] that arises from both curvature and chirality and causes difference in transition energies for mod 1 and mod 2 types. It also depends on  $d_t$ . Hence, the  $d_t$  term in the empirical equation can account the effects. The fourth factor is “many body effect” (electron-electron interaction) or “self-energy and excitonic effect” [28] that causes “ratio problem” and “blue shift problem”. This effect is adjusted within numerical fitting parameters. Since the nature and amount of these effects are still being discussed in literatures and also much disputed, any pre-defined or specific term cannot be included

to explain these effects.  $E_{11}$  and  $E_{22}$  calculated from Equations (2) and (3) deviates up to 25% from experimentally observed value if  $\gamma_0$  is considered as constant [40]. Another experimental observation is, with comparable diameter, transition energies for mod 1 type semiconducting SWCNTs are smaller than mod 2 type for odd transitions, but higher for even transitions [65], *i.e.*,  $E_{11}^{mod1} < E_{11}^{mod2}$  but  $E_{22}^{mod1} > E_{22}^{mod2}$ . Equations (2) and (3) cannot reflect this observation also. Many authors tried to improve TB model theoretically to give better prediction of experimental observations. Some of them proposed to add extra terms with Equations (2) and (3) to reflect curvature effect in terms of  $d_t$  and chirality effects in terms of chiral angle,  $\theta$  [15,48,61,62]. By including  $\cos(3\theta)$  term, these nonlinear scaling relations showed good match between experimental and calculated optical transition energies [48,66]. However, one common factor to express chirality effect in all the above-mentioned theoretical and empirical equations is a specific term  $\cos(3\theta)$  only [15,38,62] and did not consider any other combination of chiral indices. Therefore, the objective of the proposed equations is to express the optical transition energies in terms of  $d_t$  and  $(n, m)$ .

The overall issues are addressed empirically by including “curvature effect”, “chirality effect”, “trigonal warping effect”, and “many body effect” in  $\gamma_0$ , instead of directly adding those with TB model, such that the basic form of TB model remains intact. Therefore, Equations (2) and (3) may be improved by taking  $\gamma_0$  as a curvature and chirality dependent parameter, *i.e.*, including all these observed effects in  $\gamma_0$  so as to predict experimental values accurately. After following experimental values of  $E_{11}$  and  $E_{22}$  for a large number of semiconducting SWCNTs [32–43], it is found that they are very sensitive to a specific chiral index combination  $(2n - m)$ . Based on this observation and taking some insights from equations proposed by other authors [37,40,50,61,64] to improve Equations (2) and (3), the following set of empirical equations for  $\gamma_0$  and  $(r\gamma_0)$  is formulated to predict  $E_{11}$  and  $E_{22}$  of semiconducting SWCNTs with higher accuracy.

To calculate  $E_{11}$  for mod 1 type:

$$\gamma_0 = \left\{ 4.1 + \frac{5.9 - d_t}{2n - m} - \frac{1.1}{d_t} \right\} \quad (4)$$

To calculate  $E_{11}$  for mod 2 type :

$$\gamma_0 = \left\{ 3.8 - \frac{4.0 - d_t}{2n - m} + \frac{d_t}{30} \right\} \quad (5)$$

To calculate  $E_{22}$  for mod 1 type :

$$(r.\gamma_0) = \left\{ 6.85 - \frac{9.5 - d_t}{2n - m} + \frac{d_t}{8.2} \right\} \quad (6)$$

To calculate  $E_{22}$  for mod 2 type :

$$(r.\gamma_0) = \left\{ 7.5 + \frac{8.2 - d_t}{2n - m} - \frac{2.4}{d_t} \right\} \quad (7)$$

In these empirical expressions [Equations (4)–(7)] of  $\gamma_0$  and  $r\gamma_0$ , “curvature effect”, “chirality effect”, “trigonal warping effect”, and “self-energy and excitonic effect” are included by arranging nanotube diameter,  $d_t$ , and a term,  $(2n - m)$ , with numerical fitting parameters. Separate equations are proposed

for mod 1 and mod 2 types to reflect their relative difference in transition energies and also to trace their unique trends.

All the semiconducting SWCNTs that fall within theoretically possible minimum and maximum diameter range were considered. Values of the first and second optical transition energies (eV) corresponding to all these semiconducting SWCNTs were recorded from multiple reports of different optical spectroscopic experiments [14,16,33–39,41–45,50,65]. First and second optical transition energies ( $E_{11}$  and  $E_{22}$ ) of all 212 semiconducting SWCNTs for mod 1 and mod 2 types were calculated from Equations (2), (4), and (5) and Equations (3), (6), and (7), respectively. The calculated  $E_{11}$  and  $E_{22}$  showed excellent match from lowest diameter (0.4 nm) to highest diameter (3 nm). The plots of  $E_{11}$  vs.  $d_t$  and  $E_{22}$  vs.  $d_t$  for both mod 1 and mod 2 types are shown in Figure 1. The calculated values of  $E_{11}$  and  $E_{22}$  from Equations (2) and (3) provides the almost same level of accuracy with experimental results over the full diameter range. The absolute deviations (errors) of empirical data of  $E_{11}$  and  $E_{22}$  from experimental data that reduce more for increasing diameters, are shown in Figure 2. The agreement between experimental and empirical graphs over the full diameter range is so good as if they are replica of each other.

**Figure 1.** Plot of first ( $E_{11}$ ) and second ( $E_{22}$ ) optical transition energy vs. nanotube diameter ( $d_t$ ). (a) Comparing experimental and empirical  $E_{11}$  for mod 1; (b) Comparing experimental and empirical  $E_{11}$  for mod 2; (c) Comparing experimental and empirical  $E_{22}$  for mod 1; (d) Comparing experimental and empirical  $E_{22}$  for mod 2.

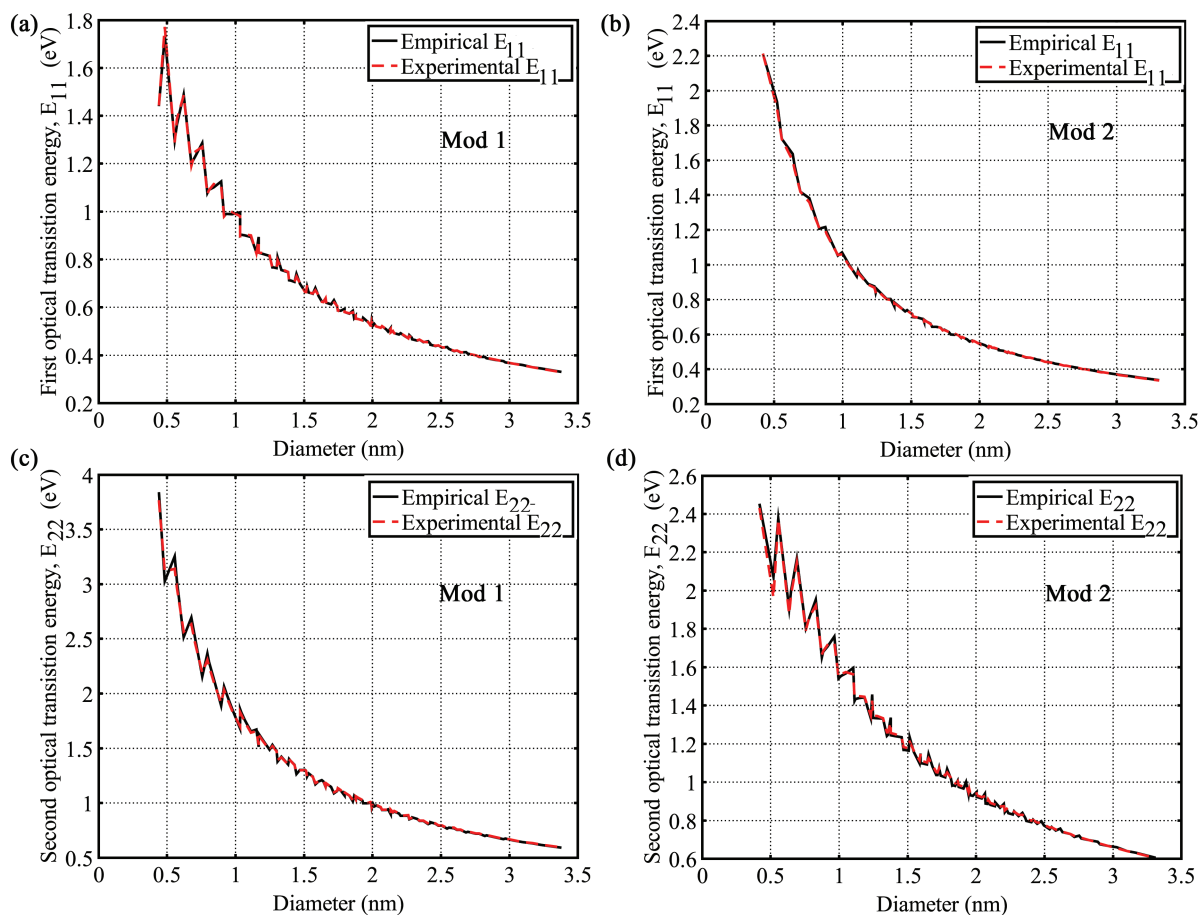
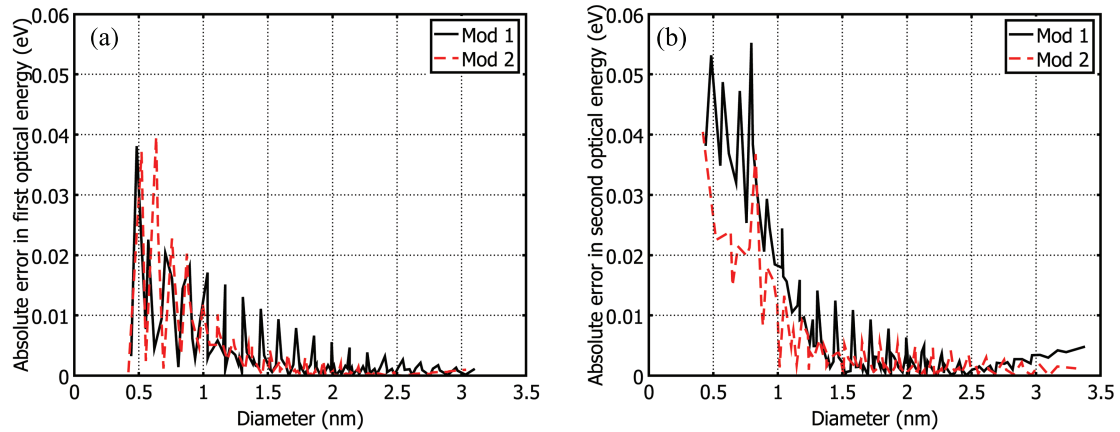


**Figure 2.** Plot of absolute deviations (errors) of first ( $E_{11}$ ) and second ( $E_{22}$ ) optical transition energy vs. nanotube diameter ( $d_t$ ). (a) Absolute deviations of empirical  $E_{11}$  from experimental data for both mod 1 and mod 2; (b) Absolute deviations of empirical  $E_{22}$  from experimental data for both mod 1 and mod 2.



The overall comparison between the empirical data and experimental data is summarized in Table 1 and Table 2 for  $E_{11}$  and  $E_{22}$ , respectively. Table 1 shows that average absolute deviations ( $|\Delta E|$ ) and % average absolute deviations ( $\% |\Delta E|$ ) of empirical data for  $E_{11}$  are very low and within tolerable margin. Average error for  $E_{11}$  over full diameter range is only 0.0036 eV (0.43%) and 0.0033 eV (0.32%) for mod 1 and mod 2, respectively. Same things can be noticed from Table 2, where average error for  $E_{22}$  over full diameter range is only 0.0113 eV (0.65%) and 0.0081 eV (0.56%) for mod 1 and mod 2, respectively. In both cases,  $|\Delta E|$  and  $\% |\Delta E|$  reduces more for increasing diameters as shown in Tables 1 and 2.

**Table 1.** Comparison of experimental and empirical data of  $E_{11}$  and corresponding average error and % average error.

Diameter, $d_t$ (nm)	MOD 1 Type		MOD 2 Type	
	Average $ \Delta E $	Average $\%  \Delta E $	Average $ \Delta E $	Average $\%  \Delta E $
$0.4 \leq d_t \leq 3.0$	0.0036	0.43%	0.0033	0.32%
$1.0 \leq d_t \leq 3.0$	0.0023	0.36%	0.0015	0.20%
$1.5 \leq d_t \leq 3.0$	0.0015	0.29%	0.0006	0.11%

The empirical expressions of  $\gamma_0$  and  $r\gamma_0$  enable Equations (2) and (3) to give almost accurate prediction of the first and second optical transition energies of semiconducting SWCNTs and remove its various shortcomings. Though nonlinear scaling relations that include  $\cos(3\theta)$  term provide almost same level of accuracy with this proposed empirical equations, the advantage of these equations is that it can reflect the chirality effect through chiral index ( $n, m$ ) instead of chiral angle  $\theta$ . Moreover, it gives almost same level of accuracy for lower and higher diameters and hence, strengthens the nearest neighbor tight binding model that is commonly accused for being highly inaccurate in lower diameter

tubes. Therefore, the approach of taking  $\gamma_0$  as a parameter whose value will depend on various observed effects is quite justified and will be proven more effective than similar earlier attempts. Moreover, the empirical equations can directly relate optical transition with nanotube chirality  $(n, m)$ .

**Table 2.** Comparison of experimental and empirical data of  $E_{22}$  and corresponding average error and % average error.

Diameter, $d_t$ (nm)	MOD 1 Type		MOD 2 Type	
	Average   $\Delta E$	Average %   $\Delta E$	Average   $\Delta E$	Average %   $\Delta E$
$0.4 \leq d_t \leq 3.0$	0.0115	0.66%	0.0083	0.57%
$1.0 \leq d_t \leq 3.0$	0.0052	0.46%	0.0037	0.35%
$1.5 \leq d_t \leq 3.0$	0.0037	0.39%	0.0031	0.33%

### 3. Method

The objective of proposing the empirical equations is to use these equations from reversed direction for the chirality assignment. Using experimental value of  $E_{ii}$  ( $E_{11}$  or  $E_{22}$ ) and  $d_t$ , the corresponding chiral index  $(n, m)$  of any unknown SWCNT can be determined. If  $E_{11}$  is available, Equations (2), (4), and (5) are used to find chiral index as discussed in Appendix A. The values of  $n$  from first optical transition energy for mod 1 and mod 2 are termed as  $n_1^{11}$  and  $n_2^{11}$ , respectively. From Equations (20) and (21), the values of  $n_1^{11}$  and  $n_2^{11}$  can be expressed as

$$n_1^{11} = \left\{ \frac{5a_1 + \sqrt{(4442.34d_t^2 - 3a_1^2)}}{14} \right\} \quad (8)$$

$$n_2^{11} = \left\{ \frac{5a_2 + \sqrt{(4442.34d_t^2 - 3a_2^2)}}{14} \right\} \quad (9)$$

where  $a_1$  and  $a_2$  are found from Equations (18) and (19), respectively. In the same way, the values of  $m$  from first optical transition energy for mod 1 and mod 2 are termed as  $m_1^{11}$  and  $m_2^{11}$ , respectively. From Equations (18) and (19), corresponding values of  $m_1^{11}$  and  $m_2^{11}$  are

$$m_1^{11} = 2n_1^{11} - a_1 \quad (10)$$

$$m_2^{11} = 2n_2^{11} - a_2 \quad (11)$$

Equations (8)–(11) give two integer pairs,  $(n_1^{11}, m_1^{11})$  and  $(n_2^{11}, m_2^{11})$ , which are the candidates for chiral index of unknown SWCNT.

In the same way, if  $E_{22}$  is available, Equations (3), (6), and (7) are used to find chiral index as discussed in Appendix B. The values of  $n$  from second optical transition energy for mod 1 and mod 2

are termed as  $n_1^{22}$  and  $n_2^{22}$ , respectively. From Equations (24) and (25), the values of  $n_1^{22}$  and  $n_2^{22}$  can be expressed as

$$n_1^{22} = \left\{ \frac{5b_1 + \sqrt{(4442.34d^2 - 3b_1^2)}}{14} \right\} \quad (12)$$

$$n_2^{22} = \left\{ \frac{5b_2 + \sqrt{(4442.34d^2 - 3b_2^2)}}{14} \right\} \quad (13)$$

where  $b_1$  and  $b_2$  are found from Equations (22) and (23), respectively. Similarly, the values of  $m$  from second optical transition energy for mod 1 and mod 2 are termed as  $m_1^{22}$  and  $m_2^{22}$ , respectively. From Equations (22) and (23), corresponding values of  $m_1^{22}$  and  $m_2^{22}$  are

$$m_1^{22} = 2n_1^{22} - b_1 \quad (14)$$

$$m_2^{22} = 2n_2^{22} - b_2 \quad (15)$$

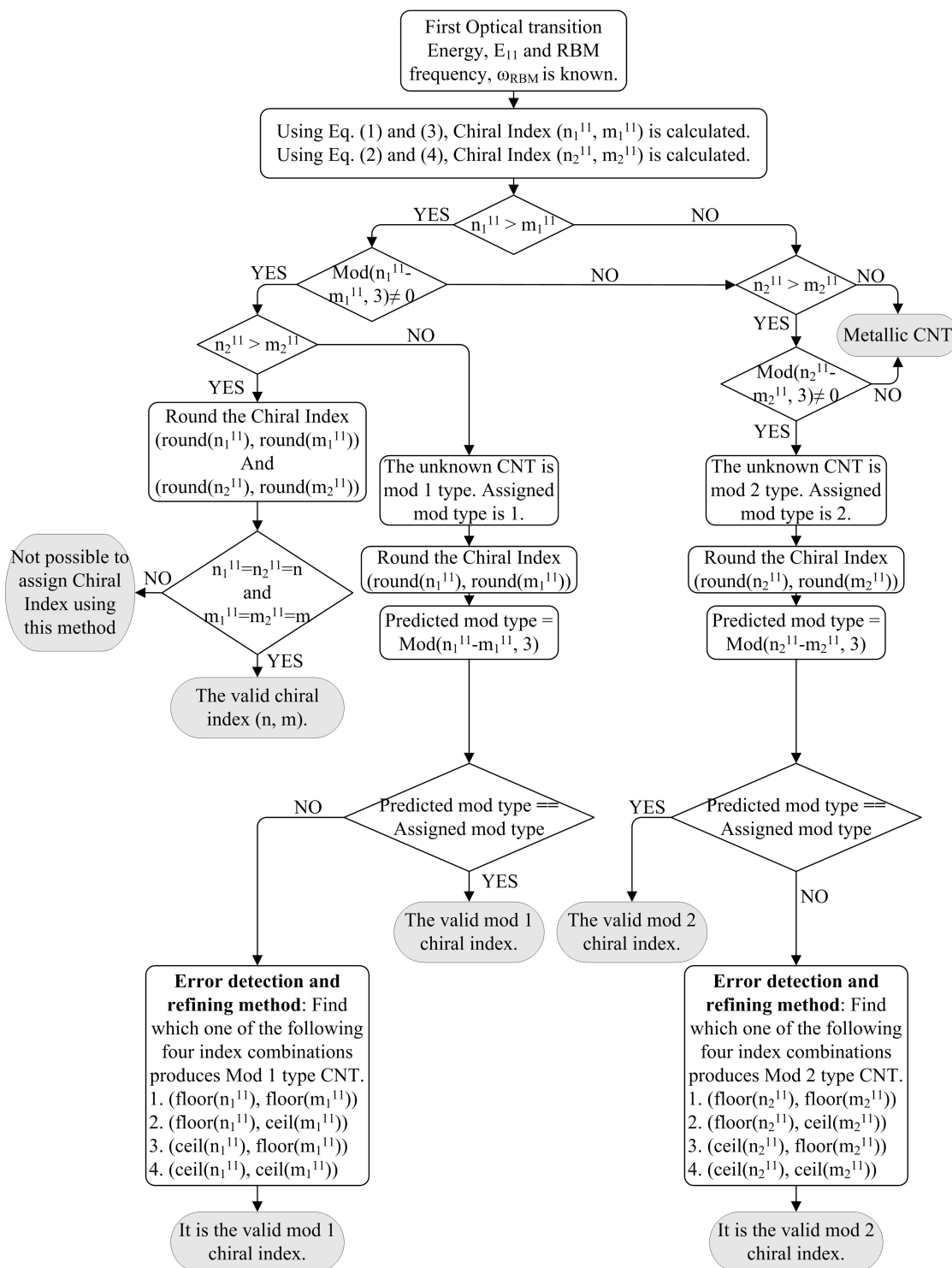
Note that the values of  $n_1^{22}$  and  $n_2^{22}$  and corresponding  $m_1^{22}$  and  $m_2^{22}$  may become fractions. Finally, Equations (12)–(15) give two pairs  $(n_1^{22}, m_1^{22})$  and  $(n_2^{22}, m_2^{22})$  that are the candidates for chiral index of unknown SWCNT.

The required two pieces of information ( $E_{11}$  or  $E_{22}$  and  $\omega_{rbm}$ ) will be taken from RRS experiments reported by numerous authors [15,16,32–43]. A flow chart of the algorithm is shown in Figure 3 for finding the chiral index  $(n, m)$  from  $E_{11}$  and  $\omega_{rbm}$ . Assuming that  $E_{11}$  and  $\omega_{rbm}$  of the unknown SWCNT from RRS experiment are known, two integer pairs  $(n_1^{11}, m_1^{11})$  and  $(n_2^{11}, m_2^{11})$  are calculated from Equations (8)–(11). The pair  $(n_1^{11}, m_1^{11})$  originates from mod 1 type's equation, whereas the pair  $(n_2^{11}, m_2^{11})$  originates from mod 2 type's equation.

Since all the samples under test are semiconducting SWCNTs, they should always satisfy  $n > m$  and  $\text{mod}(n - m, 3) \neq 0$  conditions in the proposed algorithm. The flow chart gives four distinct possibilities of values of these pairs. First, if  $n_1^{11} > m_1^{11}$  and  $n_2^{11} < m_2^{11}$ , assigned mod type is mod 1. Rounding the pair  $(n_1^{11}, m_1^{11})$ , the predicted mod type is calculated using  $\text{mod}(\text{round}(n_1^{11}) - \text{round}(m_1^{11}), 3)$ . If the assigned mod type is same as the predicted mod type, the rounded pair gives the actual mod 1 type chiral index. If the assigned mod type is not equal to the predicted mod type, error detection and refining method is applied on the  $(n_1^{11}, m_1^{11})$  pair. Second, assigned mod type is mod 2 if  $n_1^{11} < m_1^{11}$  and  $n_2^{11} > m_2^{11}$ . The predicted mod type is calculated using  $\text{mod}(n_2^{11} - m_2^{11}, 3)$  after rounding the pair  $(n_2^{11}, m_2^{11})$ . The rounded pair gives the actual mod 2 type chiral index if the assigned mod type is same as the predicted mod type. If the assigned mod type is not equal to the predicted mod type, error detection and refining method is applied on the  $(n_2^{11}, m_2^{11})$  pair. Third, for  $n_1^{11} > m_1^{11}$  and  $n_2^{11} > m_2^{11}$  conditions, if rounding to nearest interger results  $\text{round}(n_1^{11}) = \text{round}(n_2^{11}) = n$  and  $\text{round}(m_1^{11}) = \text{round}(m_2^{11}) = m$ , the chirality of the unknown CNT is  $(n, m)$ . Otherwise, the chirality of that unknown CNT cannot be determined. Finally, though the empirical equations are formulated for mod 1 and mod 2 SWCNT, it can be extended for metallic CNTs only to detect. If the unknown CNT is metallic rather than SWCNT, the values of  $(n_1^{11}, m_1^{11})$  and  $(n_2^{11}, m_2^{11})$  pairs follow the condition:  $n_1^{11} < m_1^{11}$  and  $n_2^{11} < m_2^{11}$ . Since both conditions fail to satisfy the condition of semiconducting SWCNT, the sample is a metallic CNT. This

condition is particularly useful to detect the presence of metallic CNT as clean separation of metallic CNT from semiconducting CNT is experimentally difficult.

**Figure 3.** A flow chart of the algorithm to determine the chiral index  $(n, m)$  of unknown SWCNT from RRS experiment (RBM frequency,  $\omega_{rbm}$ ) for available first optical transition energy,  $E_{11}$ . Same algorithm is used to determine chiral index for second optical transition energy,  $E_{22}$ .



In the error detection and refining method stage of the algorithm, the pair is truncated and rounded to adjust small experimental or empirical error. Since the values of  $n$  and  $m$  are estimated by rounding, the values that have fraction parts of  $n$  and  $m$  within 0.40 to 0.60 are prone to wrong assignment. Such error may come from the error margin of our empirical equations or due to slight deviation in experimental data given by RRS. If the RRS data do not deviate enough, the valid pair is in the close vicinity of the actual chiral index. Therefore, rounding such values require some tie-breaking rule. The tie-breaking rule in this method is to round down (floor) and round up (ceil). For this purpose, error detection and refining method is adopted to verify each of the assigned chirality instantly by comparing predicted mod type and assigned mod type. The possible closest chiral index pairs for mod 1 are listed as four combinations of  $(\text{floor}(n_1^{11}), \text{floor}(m_1^{11}))$ ,  $(\text{floor}(n_1^{11}), \text{ceil}(m_1^{11}))$ ,  $(\text{ceil}(n_1^{11}), \text{floor}(m_1^{11}))$ , and  $(\text{ceil}(n_1^{11}), \text{ceil}(m_1^{11}))$ . From this list, the one that matches with assigned mod type (mod 1) is reassigned as the true chiral index of that semiconducting SWCNT. Similarly, possible chiral index pairs for mod 2 are listed as four combinations and one pair is reassigned as true chiral index that matches with assigned mod type (mod 2).

The same algorithm is followed for second optical transition energy. If  $E_{22}$  and  $\omega_{rbm}$  of the unknown SWCNT from RRS experiment are known, two pairs  $(n_1^{22}, m_1^{22})$  and  $(n_2^{22}, m_2^{22})$  are calculated from Equations (12)–(15).

This method can assign the chirality of unknown semiconducting SWCNT by using only two variables:  $E_{11}$  and  $\omega_{rbm}$  or  $E_{22}$  and  $\omega_{rbm}$ . If all information is available ( $E_{11}$ ,  $E_{22}$ , and  $\omega_{rbm}$ ), this method will not provide simplified procedure for chirality assignment. Since the empirical equations for both  $E_{11}$  and  $E_{22}$  are presented here as a function of  $d_t$  and  $(n, m)$ , the ratio of optical transition energies ( $E_{11}/E_{22}$ ) is also dependent on  $d_t$  and  $(n, m)$ . In this case, the procedure for chirality assignment will be same as the the proposed algorithm. However, it will be helpful in this case to determine and verify the chiral index using this algorithm, if the chirality assignment using one data cannot be determined. As stated earlier, if the conditions  $n_1^{11} > m_1^{11}$  and  $n_2^{11} > m_2^{11}$  satisfy, but the conditions  $\text{round}(n_1^{11}) = \text{round}(n_2^{11})$  and  $\text{round}(m_1^{11}) = \text{round}(m_2^{11})$  do not satisfy, the chirality of that CNT cannot be determined using this algorithm. In this situation, alternate optical transition energy information may determine the actual chirality.

#### 4. Results

The chirality of a total of 55 semiconducting tubes has been successfully assigned using this technique, among which 28 semiconducting tubes were assigned using  $E_{11}$  and  $\omega_{rbm}$  values and 27 semiconducting tubes were assigned using  $E_{22}$  and  $\omega_{rbm}$  values. All the prediction made using the current proposed method match with the CNT determination made in the published papers. Though some assignments did not match the assigned and predicted mod type initially, the error detecting and refining method detects and corrects those assignments. Finally, the proposed technique assigned the actual chiral index to all the tested samples.

All the optical transition energy data are collected from published papers for CNTs suspended in Sodium dodecyl sulfate (SDS) solutions. It is known that environmental effect can redshift the optical transition energy. Nugraha *et al.* [67] showed that the shift of optical transition energy due to

environmental effect is related to dielectric constant of surrounding medium, nanotube diameter, subband index, and exciton size. To apply this algorithm for other surfactant, the energy shift relation [67] can be used for calculating  $E_{ii}$  for any surfactant, hence extending the algorithm of chirality assignment for any type of nanotube environment.

Table 3 shows the empirical equation based chirality assignment of 28 semiconducting SWCNTs using experimental values of  $E_{11}$  and  $\omega_{rbm}$  from reported RRS experiments [15,16,32–43]. From the table, 22 of the RRS data satisfy the conditions either  $n_1^{11} > m_1^{11}$  and  $n_2^{11} < m_2^{11} \pmod{1}$  or  $n_1^{11} > m_1^{11}$  and  $n_2^{11} < m_2^{11} \pmod{2}$ , while two of them satisfy  $\text{round}(n_1^{11}) = \text{round}(n_2^{11})$  and  $\text{round}(m_1^{11}) = \text{round}(m_2^{11})$  conditions. The remaining four semiconducting SWCNTs are further treated using error detection and refining method. For example, consider the actual chirality of (7, 3) whose  $(n, m)$  pairs are calculated as (6.7, 3.37) and (4.85, 5.4). Since these pairs satisfy the conditions  $n_1^{11} > m_1^{11}$  and  $n_2^{11} < m_2^{11}$ , the assigned mod type and the predicted chirality after rounding is 1 and (7, 3), respectively. The assigned mod type is the same as the predicted mod type (calculated from predicted chirality) in this case. Therefore, the mod type and chirality is 1 and (7, 3), respectively. Next, consider the actual chirality of (5, 4). The  $(n, m)$  pairs for mod 1 and mod 2 calculated from the empirical equations are (5.01, 3.99) and (4.83, 4.18), respectively. As rounding the values gives same pair, the assigned chirality is (5, 4). Lastly, consider the case where error detection and refining method is necessary. For the actual chirality of (13, 2), the  $(n, m)$  pairs are calculated as (8.17, 8.22) and (12.73, 2.57). These pairs satisfy the conditions  $n_1^{11} < m_1^{11}$  and  $n_2^{11} > m_2^{11}$ , and consequently, the assigned mod type and the predicted chirality after rounding is 2 and (13, 3), respectively. Here, the assigned mod type is not the same as the predicted mod type (calculated from predicted chirality) in this case. The values that have fraction parts of  $n$  and  $m$  within 0.40 to 0.60, are prone to wrong assignment due to the error margin of our empirical equations or due to slight deviation in experimental data. Therefore, the valid pair is in the close vicinity of the actual chiral index. From the four possible nearest integer pairs, (12, 2), (12, 3), (13, 2), and (13, 3), only (13, 2) is mod 2 type. Therefore, (13, 2), which has the same mod type as the assigned mod type, is considered as the correct chiral index of that SWCNT. Following the presented algorithm, all 28 semiconducting SWCNTs were properly assigned with their actual chiral index from  $E_{11}$  and  $\omega_{rbm}$ .

Table 4 shows the empirical equation based chirality assignment of 27 semiconducting SWCNTs using experimental values of  $E_{22}$  and  $\omega_{rbm}$  from reported RRS experiments [15,16,32–43]. From the table, 20 of the RRS data satisfy the conditions either  $n_1^{22} > m_1^{22}$  and  $n_2^{22} < m_2^{22} \pmod{1}$  or  $n_1^{22} > m_1^{22}$  and  $n_2^{22} < m_2^{22} \pmod{2}$ , while four of them satisfy  $\text{round}(n_1^{22}) = \text{round}(n_2^{22})$  and  $\text{round}(m_1^{22}) = \text{round}(m_2^{22})$  conditions. The remaining three semiconducting SWCNTs are further treated using error detection and refining method. Similar algorithm is applied to determine the actual chiral index from  $E_{22}$  and  $\omega_{rbm}$ .

**Table 3.** Chirality Assignment of 28 semiconducting SWCNTs from  $E_{11}$  and  $\omega_{rbm}$ . Initially, 24 of them are rightly assigned as the predicted and assigned mod type matched. The remaining four semiconducting SWCNTs are further treated using error detection and refining method.

RRS Data		$(n, m)$ pair for mod 1 <sup>a</sup>		$(n, m)$ pair for mod 2 <sup>b</sup>		Predicted chirality <sup>c</sup>	Predi- -cted <sup>d</sup>	Assi- -gned <sup>e</sup>	Re-assi- -gned <sup>f</sup>	Actual chiral
$\omega_{rbm}$ (cm <sup>-1</sup> )	$E_{11}$ (eV)	$n_1^{11}$	$m_1^{11}$	$n_2^{11}$	$m_2^{11}$	$(n, m)$	Mod	Mod	Chirality	$(n, m)$
373.0 [50]	1.488 [50]	5.01	3.99	4.83	4.18	(5, 4)	1	1		(5, 4)
335.2 [50]	1.420 [50]	5.28	4.79	6.03	3.97	(6, 4)	2	2		(6, 4)
329.5 [43]	1.249 [43]	6.7	3.37	4.85	5.4	(7, 3)	1	1		(7, 3)
309.0 [43]	1.283 [43]	6.04	4.9	5.97	4.98	(6, 5)	1	1		(6, 5)
304.0 [34]	1.362 [43]	5.5	5.65	8.84	1.47	(9, 1)	2	2		(9, 1)
297.0 [43]	1.306 [43]	5.78	5.64	7.78	3.36	(8, 3)	2	2		(8, 3)
291.0 [38]	1.100 [43]	8.75	2.32	5.28	6.37	(9, 2)	1	1		(9, 2)
283.0 [50]	1.212 [50]	6.39	5.62	7.01	4.95	(7, 5)	2	2		(7, 5)
280.0 [42]	1.110 [35]	7.85	4.11	5.79	6.36	(8, 4)	1	1		(8, 4)
263.0 [50]	1.177 [50]	6.49	6.48	9.75	2.54	(10, 3)	1	2	(10, 2)	(10, 2)
264.0 [43]	1.110 [43]	7.26	5.63	6.87	6.05	(7, 6)	1	1		(7, 6)
256.0 [37]	0.982 [50]	11.23	0.63	5.91	7.42	(11, 1)	1	1		(11, 1)
256.8 [43]	1.140 [43]	6.73	6.57	9.22	3.7	(9, 4)	2	2		(9, 4)
251.0 [50]	0.992 [50]	9.85	3.24	6.23	7.38	(10, 3)	1	1		(10, 3)
246.4 [39]	1.060 [35]	7.53	6.35	7.84	6.02	(8, 6)	2	2		(8, 6)
242.0 [42]	0.997 [50]	8.77	5.25	6.91	7.25	(9, 5)	1	1		(9, 5)
231.8 [42]	1.036 [50]	7.46	7.35	10.67	3.58	(11, 4)	1	2	(11, 3)	(11, 3)
229.0 [34]	0.979 [50]	8.41	6.57	8.04	6.96	(8, 7)	1	1		(8, 7)
226.0 [42]	0.901 [50]	11.89	2.29	6.82	8.37	(12, 2)	1	1		(12, 2)
221.8 [37]	0.904 [50]	10.74	4.34	7.19	8.32	(11, 4)	1	1		(11, 4)
215.0 [50]	0.937 [50]	8.63	7.41	9.25	6.73	(9, 7)	2	2		(9, 7)
213.4 [50]	0.898 [50]	9.81	6.24	8.01	8.17	(10, 6)	1	1		(10, 6)
210.9 [50]	0.949 [50]	8.17	8.22	12.73	2.57	(13, 3)	1	2	(13, 2)	(13, 2)
206.0 [34]	0.924 [50]	8.43	8.37	12.47	3.51	(12, 4)	2	2		(12, 4)
203.3 [39]	0.828 [50]	12.97	3.08	7.67	9.34	(13, 3)	1	1		(13, 3)
198.5 [39]	0.829 [50]	11.43	5.73	8.27	9.2	(11, 6)	2	1	(12, 5)	(12, 5)
192.5 [50]	0.841 [50]	9.78	8.25	10.27	7.73	(10, 8)	2	2		(10, 8)
187.2 [50]	0.835 [50]	9.49	9.12	12.82	5.26	(13, 5)	2	2		(13, 5)

<sup>a</sup> Using Equations (8) and (10); <sup>b</sup> Using Equations (9) and (11); <sup>c</sup> After satisfying the conditions,  $n > m$  and  $\text{mod}(n - m, 3) \neq 0$ ; <sup>d</sup> Mod type is predicted from predicted chirality; <sup>e</sup> If the predicted chirality comes from  $(n_1^{11}, m_1^{11})$  pair and  $(n_2^{11}, m_2^{11})$  pair, the assigned mod type is mod 1 and mod 2, respectively; <sup>f</sup> If the predicted mod type and assigned mod type is not same, chiral index is selected from four index combination using error detection and refining method.

Although the algorithm is presented for chirality assignment of semiconducting SWCNTs, it can also detect the presence of any possible metallic CNTs. In practice, it is not easy to separate the metallic CNTs from semiconducting CNTs completely. Therefore, the detection of metallic CNTs using the algorithm is more helpful. For example, consider the metallic CNTs having chiral index of (8, 5),  $\omega_{rbm}$  of 262.7, and optical transition energy of 2.47 eV. Using the algorithm, two pairs (4.62, 8.20) and (3.96, 8.74) are

calculated from Equations (8)–(11). Since both pairs follow the conditions,  $n_1^{11} < m_1^{11}$  and  $n_2^{11} < m_2^{11}$ , the sample is detected as metallic CNTs.

**Table 4.** Chirality Assignment of 27 semiconducting SWCNTs from  $E_{22}$  and  $\omega_{rbm}$ . Initially, 24 of them are rightly assigned as the predicted and assigned mod type matched. The remaining three semiconducting SWCNTs are further treated using error detection and refining method.

RRS Data		$(n, m)$ pair for mod 1 <sup>a</sup>		$(n, m)$ pair for mod 2 <sup>b</sup>		Predicted chirality <sup>c</sup>	Predicted <sup>d</sup>	Assigned <sup>e</sup>	Re-assigned <sup>f</sup>	Actual chirality
$\omega_{rbm}$ (cm <sup>-1</sup> )	$E_{22}$ (ev)	$n_1^{22}$	$m_1^{22}$	$n_2^{22}$	$m_2^{22}$	$(n, m)$	Mod	Mod	Chirality	$(n, m)$
309.0 [38]	2.180 [38]	6.01	4.94	5.44	5.52	(6, 5)	1	1		(6, 5)
304.0 [34]	1.800 [42]	5.07	6.07	9.22	0.83	(9, 1)	2	2		(9, 1)
299.0 [38]	1.860 [38]	5.33	6.03	7.71	3.35	(8, 3)	2	2		(8, 3)
283.0 [50]	1.920 [42]	6.01	6.01	6.69	5.34	(7, 5)	2	2		(7, 5)
278.8 [43]	2.110 [42]	7.62	4.45	5.69	6.51	(8, 4)	1	1		(8, 4)
264.6 [39]	1.690 [39]	5.93	6.95	9.98	2.09	(10, 2)	2	2		(10, 2)
264.2 [37]	1.910 [37]	6.98	5.92	6.54	6.38	(7, 6)	1	1		(7, 6)
257.5 [39]	1.720 [39]	6.31	6.95	8.55	4.51	(9, 5)	1	2	(9, 4)	(9, 4)
245.0 [42]	1.720 [42]	6.98	6.99	7.92	6.02	(8, 6)	2	2		(8, 6)
242.0 [42]	1.850 [42]	8.66	5.37	6.69	7.46	(9, 5)	1	1		(9, 5)
236.0 [50]	1.556 [50]	6.65	7.88	12.24	0.69	(12, 1)	2	2		(12, 1)
233.0 [50]	1.565 [50]	6.84	7.89	11.04	2.95	(11, 3)	2	2		(11, 3)
230.0 [42]	1.700 [42]	8.08	6.85	7.63	7.31	(8, 7)	1	1		(8, 7)
227.0 [50]	1.820 [37]	11.88	2.21	6.76	8.37	(12, 2)	1	1		(12, 2)
226.0 [46]	1.570 [46]	7.29	7.93	9.77	5.22	(10, 5)	2	2		(10, 5)
221.8 [37]	1.760 [37]	11.16	3.77	7.04	8.47	(11, 4)	1	1		(11, 4)
216.0 [39]	1.564 [39]	8.20	7.74	8.68	7.25	(9, 7)	2	2		(9, 7)
212.0 [42]	1.640 [50]	9.98	6.16	7.74	8.55	(10, 6)	1	1		(10, 6)
207.1 [46]	1.447 [46]	7.85	8.85	11.9	4.21	(12, 4)	2	2		(12, 4)
204.0 [37]	1.535 [37]	9.36	7.65	8.64	8.39	(9, 8)	1	1		(9, 8)
203.0 [42]	1.620 [42]	12.49	3.83	7.73	9.31	(12, 4)	2	1	(13, 3)	(13, 3)
200.0 [34]	1.440 [34]	8.45	8.88	10.66	6.51	(11, 7)	1	2	(11, 6)	(11, 6)
197.7 [46]	1.560 [46]	11.73	5.44	8.12	9.42	(12, 5)	1	1		(12, 5)
192.5 [50]	1.428 [50]	9.28	8.78	9.94	8.08	(10, 8)	2	2		(10, 8)
189.3 [46]	1.479 [46]	11.42	6.77	8.72	9.66	(11, 7)	1	1		(11, 7)
183.0 [34]	1.466 [34]	14.14	4.00	8.63	10.40	(14, 4)	1	1		(14, 4)
183.3 [50]	1.390 [50]	10.27	8.74	9.88	9.15	(10, 9)	1	1		(10, 9)

<sup>a</sup> Using Equations (12) and (14); <sup>b</sup> Using Equations (13) and (15); <sup>c</sup> After satisfying the conditions,  $n > m$  and  $\text{mod}(n - m, 3) \neq 0$ ; <sup>d</sup> Mod type is predicted from predicted chirality; <sup>e</sup> If the predicted chirality comes from  $(n_1^{22}, m_1^{22})$  pair and  $(n_2^{22}, m_2^{22})$  pair, the assigned mod type is mod 1 and mod 2, respectively; <sup>f</sup> If the predicted mod type and assigned mod type is not same, chiral index is selected from four index combination using error detection and refining method.

## 5. Conclusions

The empirical equation based chirality assignment presents a novel technique of assigning SWCNT chirality by solving a set of empirical equations. A set of effective empirical equations for tight binding model hopping parameter is proposed to predict first and second optical transition energies ( $E_{11}$  and  $E_{22}$ ). All the empirical equations contain a term  $(2n - m)$  to reflect the “chirality effect”. Using values of RBM frequency and any one of the first or second optical transition energies ( $E_{11}$  or  $E_{22}$ ) from RRS, the empirical equations for the  $(2n - m)$  term are solved to provide the chiral index of the unknown semiconducting SWCNT. In total, 28 semiconducting SWCNTs were assigned using  $E_{11}$  and  $\omega_{rbm}$  values and another 27 semiconducting SWCNT were assigned using  $E_{22}$  and  $\omega_{rbm}$  values. Moreover, the procedure for the detection of metallic CNTs using the algorithm is also presented.

Unlike existing methods of chirality assignment, this technique does not require graphical comparison or pattern recognition between existing experimental plot and theoretical plot. The technique is especially useful for determining chirality of isolated nanotube that does not get the advantage of pattern recognition from a produced batch of SWCNTs. This technique of chirality assignment also validates the empirical equations of band gap energy,  $E_{11}$  and  $E_{22}$  that were used to assign chirality by accessing them from reverse direction. Though the chirality assignments of some of the samples were detected and refined for the erroneous cases, there remains the possibility of obtaining truly ambiguous results from this method in some cases. In fact, so far no single proposed method for chirality assignment can be independent, and this technique may also generate some ambiguous cases that require verification by other methods. Therefore, our proposed technique for chirality assignment should also be taken under that perspective. In the future, further attempts may be taken to make this method more effective as well as to extend it to the chirality assignment of metallic CNTs.

## Appendix

### A. Chirality Assignment from First Optical Transition Energy

The relation of RRS given  $\omega_{rbm}$  with SWCNT diameter ( $d_t$ ) is established by semi-empirical equation,  $\omega_{rbm} = 223.5/d_t + 12.5$ , as proposed by many authors [16,33,34,50]. This relation gives

$$d_t = \frac{223.5}{\omega_{rbm} - 12.5} \quad (16)$$

For  $a_{cc}=0.144$  nm, using the known expression of  $d_t = \sqrt{3(n^2 + nm + m^2)} a_{cc}/\pi$ , we get,

$$n^2 + m^2 + nm = 158.655d_t^2 \quad (17)$$

As it is not known at this point whether the sample under test is mod 1 or mod 2 type, both Equations (4) and (5) are considered to find the value of  $2n - m$  in terms of  $d_t$  and  $E_{11}$ . Equations (2) and (4) give,

$$2n - m = \left\{ \frac{5.9 - d_t}{(1.1/d_t) - 4.1 + (E_{11}d_t/0.288)} \right\} = a_1(\text{say}) \quad (18)$$

and Equations (2) and (5) give,

$$2n - m = \left\{ \frac{4.0 - d_t}{(d_t/30) + 3.8 - (E_{11}d_t/0.288)} \right\} = a_2(\text{say}) \quad (19)$$

Using the value of  $\omega_{rbm}$  and  $E_{11}$  from RRS experiment, the right hand sides of Equations (17)–(19) can be known. The values of  $n$  from the first optical transition energy for mod 1 and mod 2 is termed as  $n_1^{11}$  and  $n_2^{11}$ , respectively. Solving Equations (17) and (18) for  $n_1^{11}$  gives

$$n_1^{11} = \left\{ \frac{5a_1 \pm \sqrt{(4442.34d_t^2 - 3a_1^2)}}{14} \right\} \quad (20)$$

Similarly, solving Equations (17) and (19) for  $n_2^{11}$  gives

$$n_2^{11} = \left\{ \frac{5a_2 \pm \sqrt{(4442.34d_t^2 - 3a_2^2)}}{14} \right\} \quad (21)$$

Each of the above two expressions of  $n_1^{11}$  and  $n_2^{11}$  gives two values for (+) and (-) terms. The values of  $n_1^{11}$  and  $n_2^{11}$  corresponding to the (-) terms of the above two expressions were always found to give negative value and hence become invalid as the chirality index ( $n$  and  $m$ ) cannot be negative. So, only the values of  $n_1^{11}$  and  $n_2^{11}$  corresponding to the (+) terms can be taken for consideration.

From Equations (18) and (19), the corresponding values of  $m_1^{11}$  and  $m_2^{11}$  are  $m_1^{11} = 2n_1^{11} - a_1$  and  $m_2^{11} = 2n_2^{11} - a_2$ , respectively. As the values of  $n_1^{11}$  and  $n_2^{11}$  and the corresponding  $m_1^{11}$  and  $m_2^{11}$  may become fractions, they are rounded to nearest integers. These give two integer pairs ( $n_1^{11}, m_1^{11}$ ) and ( $n_2^{11}, m_2^{11}$ ) who are the candidates for chiral index of unknown SWCNT.

## B. Chirality assignment from Second Optical Transition Energy

Just like before, as it is not known at this point whether the sample under test is mod 1 or mod 2, both Equations (16) and (17) are considered to find the value of  $2n - m$  in terms of  $d_t$  and  $E_{22}$ . Equations (3) and (6) yield

$$2n - m = \left\{ \frac{9.5 - d_t}{(d_t/8.2) + 6.85 - (E_{22}d_t/0.288)} \right\} = b_1(\text{say}) \quad (22)$$

and Equations (3) and (7) give

$$2n - m = \left\{ \frac{8.2 - d_t}{(2.4/d_t) - 7.5 + (E_{22}d_t/0.288)} \right\} = b_2(\text{say}) \quad (23)$$

Using the value of  $\omega_{rbm}$  and  $E_{22}$  from RRS experiment, the right hand sides of Equations (17), (22), and (23) can be known. The values of  $n$  from the second optical transition energy for mod 1 and mod 2 is termed as  $n_1^{22}$  and  $n_2^{22}$ , respectively. Solving Equations (17) and (22) for  $n_1^{22}$  gives

$$n_1^{22} = \left\{ \frac{5b_1 \pm \sqrt{(4442.34d_t^2 - 3b_1^2)}}{14} \right\} \quad (24)$$

Similarly, solving Equations (17) and (23) for  $n_2^{22}$  gives

$$n_2^{22} = \left\{ \frac{5b_2 \pm \sqrt{(4442.34d_t^2 - 3b_2^2)}}{14} \right\} \quad (25)$$

Again, each of the above two expressions of  $n_1^{22}$  and  $n_2^{22}$  gives two values for the (+) and (-) terms. Just like before, the values of  $n_1^{22}$  and  $n_2^{22}$  corresponding to the (-) terms of the above two expressions were always found to give negative value and become invalid. Only the values of  $n_1^{22}$  and  $n_2^{22}$  corresponding to the (+) terms can be taken.

From Equations (22) and (23), the corresponding values of  $m_1^{22}$  and  $m_2^{22}$  are  $m_1^{22} = 2n_1^{22} - b_1$  and  $m_2^{22} = 2n_2^{22} - b_2$ , respectively. As the values of  $n_1^{22}$  and  $n_2^{22}$  and the corresponding  $m_1^{22}$  and  $m_2^{22}$  may become fractions, they are rounded to nearest integers. These give two integer pairs  $(n_1^{22}, m_1^{22})$  and  $(n_2^{22}, m_2^{22})$  who are the candidates for chiral index of unknown SWCNT.

## References

1. Chen, C.X.; Lu, Y.; Kong, E.S.; Zhang, Y. F.; Lee, S.T. Nanowelded carbon-nanotube-based solar microcells. *Small* **2008**, *4*, 1313–1318.
2. Lee, J.U. Photovoltaic effect in ideal carbon nanotube diodes. *Appl. Phys. Lett.* **2005**, *87*, 073101.
3. Lu, S.; Panchapakesan, B. Photoconductivity in single wall carbon nanotube sheets. *Nanotechnology* **2006**, *17*, 1843–1850.
4. Blackburn, J.L.; Barnes, T.M.; Beard, M.C.; Kim, Y.H.; Tenent, R.C.; McDonald, T.J.; To, B.; Coutts, T.J.; Heben, M.J. Transparent conductive single-walled carbon nanotube networks with precisely tunable ratios of semiconducting and metallic nanotubes. *ACS Nano*. **2008**, *2*, 1266–1274.
5. Bindl, D.J.; Arnold, M.S. Semiconducting carbon nanotube photovoltaic photodetectors. *Int. J. High Speed Electron. Syst.* **2011**, *20*, 687.
6. Bindl, D.J.; Safron, N.S.; Arnold, M.S. Dissociating excitons photogenerated in semiconducting carbon nanotubes at polymeric photovoltaic heterojunction interfaces. *ACS Nano*. **2010**, *4*, 5657–5664.
7. Avouris, P.; Freitag, M.; Perebeinos, V. Carbon-nanotube photonics and optoelectronics. *Nat. Photon.* **2008**, *2*, 341–350.
8. Avouris, P.; Chen, J. Nanotube electronics and optoelectronics. *Mater. Today* **2006**, *9*, 46–54.
9. Fuhrer, M.S.; Kim, B.M.; Durlkop, T.; Brintlinger, T. High-mobility nanotube transistor memory. *Nano Lett.* **2002**, *2*, 755–759.
10. Javey, A.; Guo, J.; Wang, Q.; Lundstrom, M.; Dai, H.J. Ballistic carbon nanotube field-effect transistors. *Nature* **2003**, *424*, 654–657.
11. Barone, P.W.; Baik, S.; Heller, D.A.; Strano, M.S. Near-infrared optical sensors based on single-walled carbon nanotubes. *Nat. Mater.* **2005**, *4*, 86–92.
12. Hamada, N.; Sawada, S.I.; Oshiyama, A. New one-dimensional conductors: Graphitic microtubules. *Phys. Rev. Lett.* **1992**, *68*, 1579–1581.
13. Zeng, H.; Hu, H.F.; Wei, J.W.; Wang, Z.Y.; Wang, L.; Peng, P. Curvature effects on electronic properties of small radius nanotube. *Appl. Phys. Lett.* **2007**, *91*, 033102.
14. Lim, Y.; Yee, K.; Kim, J.; Hároz, E.H.; Shaver, J.; Kono, J.; Doorn, S.K.; Hauge, R.H.; Smalley, R.E. Chirality assignment of micelle-suspended single-walled carbon nanotubes using coherent phonon oscillations. *J. Korean Phys. Soc.* **2007**, *51*, 306–311.
15. Thomsen, C.; Telg, H.; Maultzsch, J.; Reich, S. Chirality assignments in carbon nanotubes based on resonant Raman scattering. *Phys. Stat. Sol. B* **2005**, *242*, 1802–1806.

16. Strano, M.S.; Doorn, S.K.; Haroz, E.H.; Kittrell, C.; Hauge, R.H.; Smalley, R.E. Assignment of  $(n, m)$  Raman and optical features of metallic single-walled carbon nanotubes. *Nano Lett.* **2003**, *3*, 1091–1096.
17. Krupke, R.; Hennrich, F.; von Lohneysen, H.; Kappes, M.M. Separation of metallic from semiconducting single-walled carbon nanotubes. *Science* **2003**, *301*, 344–347.
18. Mattsson, M.; Gromov, A.; Dittmer, S.; Eriksson, E.; Nerushev, O.A.; Campbell, E.E.B. Dielectrophoresis-induced separation of metallic and semiconducting single-wall carbon nanotubes in a continuous flow microfluidic system. *J. Nanosci. Nanotechnol.* **2007**, *7*, 3431–3435.
19. Ghosh, S.; Bachilo, S.M.; Weisman, R.B. Advanced sorting of single-walled carbon nanotubes by nonlinear density-gradient ultracentrifugation. *Nat. Nanotechnol.* **2010**, *5*, 443–450.
20. Arnold, M.S.; Stupp, S.I.; Hersam, M.C. Enrichment of single-walled carbon nanotubes by diameter in density gradients. *Nano Lett.* **2005**, *5*, 713–718.
21. Hennrich, F.; Moshhammer, K.; Kappes, M.M. Separation of metallic from semiconducting single walled carbon nanotubes by size exclusion chromatography. *Nat. Nanotechnol.* **2009**, *344*, 76128.
22. Duesberg, G.S.; Muster, J.; Krstic, V.; Burghard, M.; Roth, S. Chromatographic size separation of single-walled carbon nanotubes. *Appl. Phys. A* **1998**, *67*, 117–119.
23. Tanaka, T.; Jin, H.; Miyata, Y.; Fujii, S.; Suga, H.; Naitoh, Y.; Minari, T.; Miyadera, T.; Tsukagoshi, K.; Kataura, H. Simple and scalable gel-based separation of metallic and semiconducting carbon nanotubes. *Nano Lett.* **2009**, *9*, 1497–1500.
24. Tu, X.; Manohar, S.; Jagota, A.; Zheng, M. DNA sequence motifs for structure-specific recognition and separation of carbon nanotubes. *Nature* **2009**, *460*, 250–253.
25. Hwang, J.Y.; Nish, A.; Doig, J.; Douven, S.; Chen, C.W.; Chen, L.C.; Nicholas, R.J. Polymer structure and solvent effects on the selective dispersion of single-walled carbon nanotubes. *J. Am. Chem. Soc.* **2008**, *130*, 3543–3553.
26. Voggu, R.; Rao, K.V.; George, S.J.; Rao, C.N.R. A simple method of separating metallic and semiconducting single-walled carbon nanotubes based on molecular charge transfer. *J. Am. Chem. Soc.* **2010**, *132*, 5560–5561.
27. Dyke, C.A.; Tour, J.M. Covalent functionalization of single-walled carbon nanotubes for materials applications. *J. Phys. Chem. A* **2004**, *108*, 11151–11159.
28. Ghosh, S.; Rao, C.N.R. Separation of metallic and semiconducting single-walled carbon nanotubes through fluororous chemistry. *Nano Res.* **2009**, *2*, 183–191.
29. Qin, C.; Peng, L.M. Measurement accuracy of the diameter of a carbon nanotube from TEM images. *Phys. Rev. B* **2002**, *65*, 155431.
30. Venema, L.C.; Meunier, V.; Lambin, Ph.; Dekker, C. Atomic structure of carbon nanotubes from scanning tunneling microscopy. *Phys. Rev. B* **2000**, *61*, 2991–2996.
31. Odom, T.W.; Huang, J.L.; Lieber, C.M. STM studies of single-walled carbon nanotubes. *J. Phys. Condens. Matter* **2002**, *14*, R145–R167.
32. Herrera, J.E.; Balzano, L.; Pompeo, F.; Resasco, D.E. Raman characterization of single wall nanotubes of various diameters obtained by catalytic disproportionation of CO. *J. Nanosci. Nanotech.* **2003**, *3*, 133–138.

33. Yu, Z.; Brus, L.E. ( $n$ ,  $m$ ) structural assignments and chirality dependence in single-wall carbon nanotube Raman scattering. *J. Phys. Chem. B* **2001**, *105*, 6831–6837.
34. doorn, S.K.; Heller, D.A.; Barone, P.W.; Usrey, M.L.; Strano, M.S. Resonant Raman excitation profiles of individually dispersed single walled carbon nanotubes in solution. *Appl. Phys. A* **2004**, *78*, 1147–1155.
35. Wang, Z.; Zhao, H.; Mazumdar, S. Quantitative calculations of the excitonic energy spectra of semiconducting single-walled carbon nanotubes within a  $\pi$ -electron model. *Phys. Rev. B* **2006**, *74*, 195406.
36. Telg, H.; Maultzsch, J.; Reich, S.; Hennrich, F.; Thomsen, C. Chirality distribution and transition energies of carbon nanotubes. *Phys. Rev. Lett.* **2004**, *93*, 177401.
37. Maultzsch, J.; Telg, H.; Reich, S.; Thomsen, C. Radial breathing mode of single-walled carbon nanotubes optical transition energies and chiral-index assignment. *Phys. Rev. B* **2005**, *72*, 205438.
38. Jorio, A.; Santos, A.P.; Ribeiro, H.B.; Fantini, C.; Souza, M.; Vieira, J.P.M.; Furtado, C.A.; Jiang, J.; Saito, R.; Balzano, L.; *et al.* Quantifying carbon-nanotube species with resonance Raman scattering. *Phys. Rev. B* **2005**, *72*, 075207.
39. Telg, H.; Maultzsch, J.; Reich, S.; Hennrich, F.; Thomsen, C. Raman excitation profiles for the ( $n_1$ ,  $n_2$ ) assignment in carbon nanotubes. *AIP Conf. Proc.* **2004**, *723*, 330.
40. Weisman, R.B.; Bachilo, S.M. Dependence of optical transition energies on structure for single-walled carbon nanotubes in aqueous suspension: An empirical katura plot. *Nano Lett.* **2003**, *3*, 1235–1238.
41. Dresselhaus, M.S.; Dresselhaus, G.; Jorio, A.; Filho, A.G.S.; Saito, R. Raman spectroscopy on isolated single wall carbon nanotubes. *Carbon* **2002**, *40*, 2043–2061.
42. Fantini, C.; Jorio, A.; Souza, M.; Strano, M.S.; Dresselhaus, M.S.; Pimenta, M.A. Optical transition energies for carbon nanotubes from resonant Raman spectroscopy: Environment and temperature effects. *Phys. Rev. Lett.* **2004**, *93*, 147406.
43. Telg, H.; Maultzsch, J.; Reich, S.; Thomsen, C. Resonant-Raman intensities and transition energies of the  $E_{11}$  transition in carbon nanotubes. *Phys. Rev. B* **2006**, *74*, 115415.
44. Hagen, A.; Hertel, T. Quantitative analysis of optical spectra from individual single-wall carbon nanotubes. *Nano Lett.* **2003**, *3*, 383–388.
45. Lian, Y.; Maeda, Y.; Wakahara, T.; Akasaka, T.; Kazaoui, S.; Minami, N.; Choi, N.; Tokumoto, H. Assignment of the fine structure in the optical absorption spectra of soluble single-walled carbon nanotubes. *J. Phys. Chem. B* **2003**, *107*, 12082–12087.
46. Namkung, M.; Williams, P.A.; Mayweather, C.D.; Wincheski, B.; Park, C.; Namkung, J.S. Chirality Characterization of Dispersed Single Wall Carbon Nanotubes. In *Proceedings of the NASA MRS Spring Meeting*, San Francisco, CA, USA, 28 March–1 April 2005.
47. Berciaud, S.; Cognet, L.; Poulin, P.; Weisman, R.B.; Lounisa, B. Absorption spectroscopy of individual single-walled carbon nanotubes. *Nano Lett.* **2007**, *7*, 1203–1207.
48. Araujo, P. T.; Doorn, S.K.; Kilina, S.; Tretiak, S.; Einarsson, E.; Maruyama, S.; Chacham, H.; Pimenta, M.A.; Jorio, A. Third and fourth optical transitions in semiconducting carbon nanotubes. *Phys. Rev. Lett.* **2007**, *98*, 067401.

49. Weisman, R.B. Fluorimetric characterization of single-walled carbon nanotubes. *Anal. Bioanal. Chem.* **2010**, *396*, 1015–1023.
50. Bachilo, S.M.; Strano, M.S.; Kittrell, C.; Hauge, R.H.; Smalley, R.E.; Weisman, R.B. Structure-assigned optical spectra of single-walled carbon nanotubes. *Science* **2002**, *298*, 2361.
51. O’Connell, M.J.; Bachilo, S.M.; Huffman, C.B.; Moore, V.C.; Strano, M.S.; Haroz, E.H.; Rialon, K.L.; Boul, P.J.; Noon, W.H.; Kittrell, C.; *et al.* Band gap fluorescence from individual single-walled carbon nanotubes. *Science* **2002**, *297*, 5581–5593.
52. Tsyboulski, D.A.; Rocha, J.D.R.; Bachilo, S.M.; Cognet, L.; Weisman, R.B. Structure-dependent fluorescence efficiencies of individual single-walled carbon nanotubes. *Nano Lett.* **2007**, *7*, 3080–3085.
53. Jones, M.; Engtrakul, C.; Metzger, W.K.; Ellingson, R.J.; Nozik, A.J.; Heben, M.J.; Rumbles, G. Analysis of photoluminescence from solubilized single-walled carbon nanotubes. *Phys. Rev. B* **2005**, *71*, 115426.
54. Sauvajol, J.L.; Anglaret, E.; Rols, S.; Alvarez, L. Phonons in single wall carbon nanotube bundles. *Carbon* **2002**, *40*, 1697–1714.
55. Venkateswaran, U.D.; Rao, A.M.; Richter, E.; Menon, M.; Rinzler, A.; Smalley, R.E.; Eklund, P.C. Probing the single-wall carbon nanotube bundle: Raman scattering under high pressure. *Phys. Rev. B* **1999**, *59*, 10928.
56. Kane, C.L.; Mele, E.J. The ratio problem in single carbon nanotube fluorescence spectroscopy. *Phys. Rev. Lett.* **2003**, *90*, 207401.
57. Correa, J.D.; da Silva, A.J.R.; Pacheco, M. Tight-binding model for carbon nanotubes from ab-initio calculations. *J. Phys. Condens. Matter* **2010**, *22*, 275503.
58. Reich, S.; Maultzsch, J.; Thomsen, C.; Ordejon, P. Tight-binding description of graphene. *Phys. Rev. B* **2002**, *66*, 035412.
59. Zólyomi, V.; Kürti, J. First-principles calculations for the electronic band structures of small diameter single-wall carbon nanotubes. *Phys. Rev. B* **2004**, *70*, 085403.
60. Popov, V.N. Curvature effects on the structural, electronic and optical properties of isolated single-walled carbon nanotubes within a symmetry-adapted non-orthogonal tight-binding model. *New J. Phys.* **2004**, *6*, 17.
61. Ding, J.W.; Yan, X.H.; Cao, J.X. Analytical relation of band gaps to both chirality and diameter of single-wall carbon nanotubes. *Phys. Rev. B* **2002**, *66*, 073401.
62. Jorio, A.; Araujo, P.; Doorn, S.K.; Maruyama, S.; Chacham, H.; Pimenta, M.A. The Kataura plot over broad energy and diameter ranges. *Phys. Stat. Sol. B* **2006**, *243*, 3117–3121.
63. Reich, S.; Thomsen, C. Chirality dependence of the density-of-states singularities in carbon nanotubes. *Phys. Rev. B* **2000**, *62*, 4273.
64. Saito, R.; Dresselhaus, G.; Dresselhaus, M.S. Trigonal warping effect of carbon nanotubes. *Phys. Rev. B* **2000**, *61*, 2981–2990.
65. Sfeir, M.Y.; Beetz, T.; Wang, F.; Huang, L.; Huang, X.M.H.; Huang, M.; Hone, J.; O’Brien, S.; Misewich, J.A.; Heinz, T.F.; *et al.* Optical spectroscopy of individual single-walled carbon nanotubes of defined chiral structure. *Science* **2006**, *312*, 554–556.

66. Liu, K.; Deslippe, J.; Xiao, F.; Capaz, R. B.; Hong, X.; Aloni, S.; Zettl, A.; Wang, W.; Bai, X.; Louie, S.G.; *et al.* An atlas of carbon nanotube optical transitions. *Nat. Nanotechnol.* **2012**, *7*, 325–329.
67. Nugraha, A.R.T.; Saito, R.; Sato, K.; Araujo, P.T.; Jorio, A.; Dresselhaus, M.S. Dielectric constant model for environmental effects on the exciton energies of single wall carbon nanotubes. *Appl. Phys. Lett.* **2010**, *97*, 091905.

© 2013 by the author; licensee MDPI, Basel, Switzerland. This article is an open access article distributed under the terms and conditions of the Creative Commons Attribution license (<http://creativecommons.org/licenses/by/3.0/>).